Contribution from the Department of Applied Chemistry, Faculty of Engineering, and the Institute of Scientific and Industrial Research, Osaka University, Yamadaoka, Suita, Osaka 565, Japan, and the Department of Material Physics, Faculty of Engineering Science, Osaka University, Toyonaka, Osaka 560, Japan

High-Pressure Synthesis, Crystal Structures, and Luminescence Properties of Europium(II) Metasilicate and Europium(II)-Activated Calcium and Strontium Metasilicates

KEN-ICHI MACHIDA,[1a] GIN-YA ADACHI,*[1a] JIRO SHIOKAWA,[1a] MASAHIKO SHIMADA,[1b] MITSUE KOIZUMI,[1b] KAICHI SUITO,[1c] and AKIFUMI ONODERA[1c]

Received August 14, 1981

High-pressure synthesis up to 150 kbar was carried out on europium(II) metasilicate, $EuSiO_3$, and Eu^{2+}-activated calcium and strontium metasilicates, $MSiO_3:Eu^{2+}$ (M = Ca or Sr), and the luminescence properties of the resulting materials were studied. The crystal structures of the host lattices, δ- and δ′-$SrSiO_3$, were determined from the three-dimensional X-ray diffraction data. New high-pressure phases, δ- and δ′-$EuSiO_3$, were obtained under pressures of about 60 and 70 kbar at 1000–1400 °C, and the atmospheric phases, α-$CaSiO_3:Eu^{2+}$ and α-$SrSiO_3:Eu^{2+}$, transformed into δ-$CaSiO_3:Eu^{2+}$, δ-$SrSiO_3:Eu^{2+}$, and δ′-$SrSiO_3:Eu^{2+}$ at 35–100 kbar and 800–1400 °C. The peak positions for the emission bands of $MSiO_3:Eu^{2+}$ shifted to short wavelength with the phase transformations: green (ca. 510 nm), α-$CaSiO_3:Eu^{2+}$; blue (ca. 470 nm), δ-$CaSiO_3:Eu^{2+}$; green (ca. 500 nm), α- and δ-$SrSiO_3:Eu^{2+}$; blue (ca. 465 nm), δ′-$SrSiO_3:Eu^{2+}$. In addition, their emission intensities were appreciably increased when the samples transformed into high-pressure phases. The phosphors, δ-$CaSiO_3:Eu^{2+}$ and δ-$SrSiO_3:Eu^{2+}$, gave quantum efficiency values of about 20 and 40%, whereas those of the atmospheric phases were around 1%. The crystals of δ- and δ′-$SrSiO_3$ belong to the triclinic system of space group $P\bar{1}$ with $Z = 6$, $a = 6.874$ (2) Å, $b = 6.894$ (2) Å, $c = 9.717$ (3) Å, $\alpha = 85.01$ (3)°, $\beta = 110.57$ (3)°, and $\gamma = 104.01$ (2)° and the monoclinic system of space group $P2_1/c$ with $Z = 8$, $a = 7.452$ (4) Å, $b = 6.066$ (2) Å, $c = 13.479$ (7) Å, and $\beta = 117.09$ (4)°, respectively. These structures were solved by the direct method and refined by block-diagonal least-squares methods. Final R values were 0.043 for 1458 observed reflections of δ-$SrSiO_3$ and 0.046 for 914 observed reflections of δ′-$SrSiO_3$, respectively. The crystal lattice of δ-$SrSiO_3$ is constructed of the same $(Si_3O_9)^{6-}$ rings as α-$SrSiO_3$, and δ′-$SrSiO_3$ consists of four-membered rings of $(Si_4O_{12})^{8-}$. The Sr atoms in δ-$SrSiO_3$ were surrounded by eight or six oxygens, while those in δ′-$SrSiO_3$ occupy the sites coordinated by eight oxygens. The above-mentioned luminescence properties are discussed on the basis of X-ray structural analyses of the host lattices and temperature dependences of the emission spectra.

Introduction

Divalent europium compounds have been synthesized because they are of interest for their magnetic and spectroscopic properties. On a series of silicates, α-$EuSiO_3$ (atmospheric form), Eu_2SiO_4, and Eu_3SiO_5, which have been obtained in the binary system EuO–SiO_2, the magnetic susceptibilities and magnetooptical properties have been studied at low temperature.[2a,b] A number of Eu^{2+}-activated compounds give line or band emissions based on the $4f^7$–$4f^7$ or $4f^7$–$4f^65d$ transitions of Eu^{2+} ions, whose peak positions and light outputs greatly depend on the constituent chemical species and crystal structures of the host lattices.[2c,d] Recently we have found that the emission intensity of $SrB_2O_4:Eu^{2+}$ drastically increases when the host lattice transforms into a high-pressure phase (δ form).[3] The luminescence properties of Eu^{2+}-activated compounds in the system M′O–SiO_2 (M = Ca, Sr, or Ba) have been investigated by some workers,[4] who have found that those silicates give band emissions of color violet-blue to green. Among them, $M'_2SiO_4:Eu^{2+}$ is a green-emitting phosphor with high quantum efficiency, and $M'SiO_3:Eu^{2+}$ has been reported to show emissions varying from violet to green, depending on the heating temperature of samples.[4a]

Alkaline-earth metasilicates show various high-temperature and high-pressure polymorphisms.[5] The calcium silicate α- or β-$CaSiO_3$ (atmospheric form) is transformed into δ-$CaSiO_3$ at about 30 kbar and 900 °C, and ε-$CaSiO_3$ is obtained above 100 kbar at 1000 °C.[6] The structure of β-$CaSiO_3$ (low-temperature form) consists of $(SiO_3)_\infty$ chains of SiO_4 tetrahedra,[7] while α-$CaSiO_3$ (high-temperature form) has been presumed to contain a $(Si_3O_9)^{6-}$ ring of three SiO_4 tetrahedra.[8] Trojer[9] has determined the structure of δ-$CaSiO_3$, of which the structural framework is the same $(Si_3O_9)^{6-}$ ring as in α-$CaSiO_3$. The ε phase crystallizes in the cubic system (perovskite type) and its structure is composed of a three-dimensional $(SiO_3)_\infty$ network of SiO_6 octahedra. The strontium metasilicate α-$SrSiO_3$ also gives two high-pressure phases at 34–120 kbar and 750–1400 °C.[10] The structure of α-$SrSiO_3$ has been found from our work[11] to consist of $(Si_3O_9)^{6-}$ rings in a similar manner as α- and δ-$CaSiO_3$, but the structural analyses of the two high-pressure phases have not been performed.

If the above-mentioned high-pressure phases of $CaSiO_3:Eu^{2+}$ and $SrSiO_3:Eu^{2+}$ are obtained, they will show various luminescence properties. Since the ionic radius of Eu^{2+} is similar to those of Ca^{2+} and Sr^{2+}, α-$EuSiO_3$ can also be expected to transform into such high-pressure forms as mentioned above. This paper reports the high-pressure synthesis of $EuSiO_3$,

(1) (a) Department of Applied Chemistry. (b) Institute of Scientific and Industrial Research. (c) Department of Material Physics.
(2) (a) Shafer, M. W. *J. Appl. Phys.* **1965**, *36*, 1145. (b) Suits, J. C.; Argyle, B. E.; Freiser, M. J. *Ibid.* **1966**, *37*, 1391. (c) Blasse, G.; Bril, A. *Philips Tech. Rev.* **1970**, *31*, 304. (d) Blasse, G. *Struct. Bonding (Berlin)* **1976**, *26*, 43–79.
(3) (a) Machida, K.; Adachi, G.; Shiokawa, J.; Shimada, M.; Koizumi, M. *J. Lumin.* **1980**, *21*, 233. (b) Machida, K.; Adachi, G.; Shiokawa, J.; Shimada, M.; Koizumi, M. *Inorg. Chem.* **1980**, *19*, 983.
(4) (a) Jenkins, H. G.; McKeag, A. H. *J. Electrochem. Soc.* **1950**, *97*, 415. (b) Blasse, G.; Wanmaker, W. L.; Ter Vrugt, J. W.; Bril, A. *Philips Res. Rep.* **1968**, *23*, 189.
(5) Toropov, N. A.; Barzakovskii, V. P.; Lapin, V. V.; Kurtseva, N. N. "Handbook of Phase Diagrams of Silicate Systems", 2nd ed.; Jerusalem, 1972; Vol. I, Binary Systems, 20–44.
(6) (a) Ringwood, A. E.; Major, A. *Earth Planet. Sci. Lett.* **1967**, *2*, 106. (b) Liu, L.; Ringwood, A. E. *Ibid.* **1975**, *28*, 209.
(7) (a) Mamedov, K. S.; Belov, N. V. *Dokl. Akad. Nauk SSSR* **1956**, *107*, 463. (b) Trojer, F. J. *Z. Kristallogr., Kristallgeom., Kristallphys. Kristallchem.* **1968**, *127*, 291.
(8) Jeffery, J. W.; Heller, L. *Acta Crystallogr.* **1953**, *6*, 807.
(9) Trojer, F. J. *Z. Kristallogr., Kristallgeom., Kristallphys. Kristallchem.* **1969**, *130*, 185.
(10) Shimizu, Y.; Syono, Y.; Akimoto, S. *High Temp.—High Pressures* **1970**, *2*, 113.
(11) Machida, K.; Adachi, G.; Shiokawa, J.; Shimada, M.; Koizumi, M. *Acta Crystallogr., Sect. B*, in press.

0020-1669/82/1321-1512$01.25/0

$CaSiO_3:Eu^{2+}$, and $SrSiO_3:Eu^{2+}$, the luminescence properties of the resulting materials, and the crystal structures of δ- and δ′-$SrSiO_3$.

Experimental Section

Sample Preparation. The atmospheric phase, α-$EuSiO_3$, was obtained by heating a mixture of appropriate amounts of Eu_2O_3 (99.99%), Si (99.999%), and SiO_2 (99.999%) at 1400 °C for 3 × 2 h (two times) in Ar. The phosphors of α-$MSiO_3:Eu^{2+}$ (M = Ca or Sr) were prepared by the following standard ceramic technique: appropriate amounts of SiO_2 and $MCO_3:Eu^{3+}$, coprecipitated from a dilute HCl solution of luminescent grade MCO_3 and Eu_2O_3 by the slow addition of a $(NH_4)_2CO_3$ solution, were fully mixed, pelletized, and heated at 1300 °C for 3 h in a reducing stream of H_2. The high-pressure treatments of samples were carried out with a cubic anvil type apparatus (60 kbar)[12] and a split-sphere type apparatus (60–150 kbar).[13] The powdered samples were packed into boron nitride cups (6 × 3.2 mm for the former apparatus or 3.5 × 4 mm for the latter one) and were heated by a graphite or a molybdenum heater. A Pt/Pt–13% Rh thermocouple was employed to measure the temperature of the sample. After the desired pressure and temperature were maintained, the samples were quenched to room temperature, and then the pressure was released.

Single crystals for the polymorphs of $SrSiO_3$ were grown from a mixture of polycrystalline α-$SrSiO_3$ containing KCl in the molar ratio $SrSiO_3$:KCl = 10:1 as a flux. The samples were subjected to the appropriate pressure at 1300 or 1400 °C for 60 min and then were allowed to cool to 800 °C at a rate of 2 °C/min. The applied pressures were 40 and 55 kbar for δ and δ′ phases, respectively. Transparent single crystals (0.3 mm long) were grown, the crystal habits of which were needles for the δ form and plates of the δ′ one. For runs, in which samples containing the larger amount of KCl than the above-mentioned ratio of $SrSiO_3$:KCl were used, an unknown phase was formed as a byproduct. The polycrystalline samples for the polymorphs of $SrSiO_3$ were obtained as follows: α-$SrSiO_3$ was prepared by heating the stoichiometric mixture of $SrCO_3$ and SiO_2 at about 1300 °C for 5 × 2 h (two times) in air, and δ- and δ′-$SrSiO_3$ were prepared from α-$SrSiO_3$ by treatments of 40 and 60 kbar at about 1000 °C.

Optical and Magnetic Susceptibility Measurements. Ultraviolet luminescence spectra of powdered samples were measured with a Shimadzu recording absolute spectrofluorophotometer, which can record the corrected excitation and emission spectra by the automatic compensation and precalibration systems for the instrumental factors. Measurements of diffuse reflection spectra were made with a Shimadzu UV-180 double-beam spectrophotometer equipped with an attachment for an integrating sphere, with optical filters cutting the emissions of samples. Magnesium oxide was used as a standard material, the reflection of which was refined as 100%. The quantum efficiencies of samples were estimated by integrating the corresponding area below curves as corrected emission spectra with reflection spectra under excitation by a xenon lamp and with reference to a suitable standard phosphor, $CaWO_4:Pb^{2+}$ (NBS 1026). The quantum efficiency under 254-nm excitation at 300 K of the $CaWO_4:Pb^{2+}$ was defined as 76%.

Magnetic susceptibility measurements were carried out with a Shimadzu MB-11 magnetic balance over a temperature range of 80–300 K.

Crystallographic Measurements. Preliminary oscillation and Weissenberg photographs (Cu Kα) showed that the crystals of δ- and δ′-$SrSiO_3$ belong to the triclinic system of $P1$ or $P\bar{1}$ and the monoclinic system of $P2_1/c$ (systematic absences: $l = 2n + 1$ for $h0l$ and $k = 2n + 1$ for $0k0$), respectively. Accurate cell parameters (Table I) were determined by least-squares treatments of the X-ray powder patterns (Cu Kᾱ: 1.5418 Å) for the polycrystalline samples, calibrated with high-purity silicon as an internal standard. The intensity data were measured on a Rigaku automated four-circle diffractometer with graphite-monochromatized Mo Kα radiation. The ω–2θ scan method was employed with a scanning rate of 4°/min. The stationary-crystal and stationary-counter background counts were measured at the beginning and end of the ω–2θ scan for 3 s on each reflection. All possible reflections were collected out to the 2θ value of 60°. Three standard reflections were monitored every 100 reflections, and no apparent decay in intensity was detected. The observed reflections with $F_o > 3\sigma_{F_o}$ (δ-$SrSiO_3$, 1458 reflections; δ′-$SrSiO_3$, 914 reflections) were obtained and were used for the later calculations. The usual Lorentz and polarization corrections were applied, but the absorption and anomalous dispersion effects for heavy atoms were not considered.

Table I. Crystal Data for δ- and δ′-$SrSiO_3$

	δ form	δ′ form
fw	163.70	163.70
symmetry	triclinic	monoclinic
space group	$P\bar{1}$	$P2_1/c$
a, Å	6.874 (2)	7.452 (4)
b, Å	6.894 (2)	6.066 (2)
c, Å	9.717 (3)	13.479 (7)
α, deg	85.01 (3)	
β, deg	110.57 (3)	117.09 (4)
γ, deg	104.01 (2)	
V, Å^3	418.3 (2)	542.5 (4)
Z	6	8
d_{measd}, g cm^{-3}	3.87	3.96
d_{calcd}, g cm^{-3}	3.90	4.01
λ, Å	0.710 69	0.710 69
μ(Mo Kα), mm^{-1}	18.946	19.481
F(000)	456	608
cryst size, mm^3	0.08 × 0.07 × 0.15	0.15 × 0.25 × 0.10

Structure Determinations and Refinements. The structures of δ- and δ′-$SrSiO_3$ were solved by a direct method (MULTAN 78 program[14]) and refined by a block-diagonal least-squares method (HBLS-V program[15]), the function minimized being $\sum w(|F_o| - |F_c|)^2$. The final positional and thermal parameters along with their estimated standard deviations are listed in Tables II and III.

For the δ form, the space group of $P\bar{1}$ gave a satisfactory result, and the coordinates of Sr atoms could be determined as follows: Sr(1) at 0.75, 0.25, 0.00; Sr(2) at 0.26, 0.08, 0.65; Sr(3) at 0.11, 0.58, 0.35. The remaining atoms (Si and O) were located on the successive difference Fourier maps. Several cycles of the refinement with anisothermal parameters for Sr atoms gave conventional R and R_w values of 0.043 and 0.077, where $R = \sum||F_o| - |F_c||/\sum|F_o|$ and $R_w = [\sum w(|F_o| - |F_c|)^2/\sum w(F_o)^2]^{1/2}$. The weighting scheme $w = (F_m/F_o)^2$ for $F_o > F_m$ (=20.0) and $w = 1.0$ for $F_o \leq F_m$ (=20.0) was employed.

The Sr atoms of δ′-$SrSiO_3$ were located at 0.26, 0.09, 0.24 for Sr(1) and 0.21, 0.90, 0.63 for Sr(2), and the coordinates of Si and O atoms were determined from the difference Fourier maps. All of these atoms occupy general positions (4e site) of space group $P2_1/c$. The values of R and R_w were finally converged to 0.046 and 0.050 by the anisotropic refinements for Sr atoms. The same weighting scheme (F_m = 30.0) as was used for δ-$SrSiO_3$ was used for the refinements. The atomic scattering factors used in all the calculations were taken from ref 16.

Results

$EuSiO_3$. Under pressures of about 60 and 70 kbar at 1000–1400 °C, α-$EuSiO_3$ transformed into two high-pressure phases, which were termed in a similar manner as calcium and strontium analogues, viz., δ- and δ′-$EuSiO_3$. This polymorphism is the same as that shown in $SrSiO_3$.

The Eu^{2+} ions tend to be easily oxidized into Eu^{3+} ions at high temperature. The magnetic properties of the resulting materials are summarized in Table IV. Since the effective magnetic moments, μ_{eff}, are in good agreement with the theoretical value (7.94 μ_B), we can consider that the ions of Eu in the samples are mainly in the divalent state. The paramagnetic Curie temperature is about −1 K for α-$EuSiO_3$ and about −3 K for δ- and δ′-$EuSiO_3$. This indicates that these

(12) Shimada, M.; Ogawa, N.; Koizumi, M.; Dachille, F.; Roy, R. *Am. Ceram. Soc. Bull.* **1979**, *58*, 519.
(13) (a) Kawai, N.; Togaya, M.; Onodera, A. *Proc. Jpn. Acad.* **1973**, *49*, 623. (b) Suito, K.; Kawai, N. *High-pressure Sci. Technol. AIRAPT Conf., 6th* **1979**, *2*, 53.
(14) Main, P.; Hull, S. E.; Lessinger, L.; Germain, G.; Declercq, J. P.; Woolfson, M. M. "A System of Computer Programs for the Automatic Solution of Crystal Structures from X-ray Diffraction Data, MULTAN 78"; University of York: York, England, 1978.
(15) Ashida, T. "The Universal Crystallographic Computing System—Osaka"; The Computation Center, Osaka University: Osaka, Japan, 1979; pp 53–59.
(16) "International Tables for X-Ray Crystallography"; Kynoch Press: Birmingham, England, 1974; Vol. IV, pp 99–101.

Table II. Positional and Thermal Parameters and Their Estimated Standard Deviations of δ-$SrSiO_3$

atom	x	y	z	U_{11}[a]	U_{22}	U_{33}	U_{12}	U_{13}	U_{23}
Sr(1)	0.752 (2)	0.250 (1)	0.003 (1)	458 (22)	274 (18)	235 (17)	−42 (15)	111 (16)	25 (14)
Sr(2)	0.262 (2)	0.079 (2)	0.652 (1)	641 (24)	515 (21)	308 (20)	349 (20)	101 (17)	98 (16)
Sr(3)	0.110 (2)	0.578 (2)	0.348 (1)	880 (27)	449 (20)	316 (20)	403 (19)	337 (18)	244 (16)

atom	x	y	z	B, Å²	atom	x	y	z	B, Å²
Si(1)	0.600 (5)	0.391 (5)	0.291 (5)	0.91 (6)	O(4)	0.473 (12)	0.386 (11)	0.129 (11)	0.87 (16)
Si(2)	0.256 (4)	0.250 (4)	0.012 (4)	0.40 (5)	O(5)	0.094 (11)	0.377 (10)	−0.079 (10)	0.54 (14)
Si(3)	0.253 (5)	0.056 (4)	0.290 (5)	0.78 (6)	O(6)	0.336 (10)	0.131 (10)	−0.082 (10)	0.45 (14)
O(1)	0.759 (10)	0.258 (10)	0.266 (10)	0.44 (14)	O(7)	0.173 (11)	0.090 (10)	0.127 (11)	0.71 (15)
O(2)	0.439 (10)	0.247 (9)	0.384 (9)	0.24 (13)	O(8)	0.371 (11)	−0.112 (10)	0.269 (10)	0.68 (15)
O(3)	0.757 (11)	0.563 (10)	0.388 (10)	0.61 (15)	O(9)	0.122 (11)	−0.053 (10)	0.389 (10)	0.58 (15)

[a] The form of the anisotropic thermal parameter (×10⁴) is $\exp[-2\pi^2(U_{11}h^2a^{*2} + U_{22}k^2b^{*2} + U_{33}l^2c^{*2} + 2U_{12}hka^*b^* + 2U_{13}hla^*c^* + 2U_{23}klb^*c^*)]$.

Table III. Positional and Thermal Parameters and Their Estimated Standard Deviations of δ′-$SrSiO_3$

atom	x	y	z	U_{11}[a]	U_{22}	U_{33}	U_{12}	U_{13}	U_{23}
Sr(1)	0.2567 (10)	0.0897 (9)	0.3404 (10)	94 (5)	39 (4)	79 (5)	1 (4)	59 (4)	7 (4)
Sr(2)	0.2147 (10)	0.8983 (10)	0.6261 (9)	77 (4)	41 (4)	65 (5)	−3 (4)	42 (4)	2 (4)

atom	x	y	z	B, Å²	atom	x	y	z	B, Å²
Si(1)	0.158 (3)	0.590 (3)	0.408 (3)	0.37 (4)	O(3)	0.054 (8)	0.829 (8)	0.400 (8)	0.37 (11)
Si(2)	0.451 (3)	0.353 (3)	0.617 (3)	0.31 (4)	O(4)	0.314 (9)	0.561 (8)	0.539 (9)	0.71 (12)
O(1)	0.311 (8)	0.590 (9)	0.346 (8)	0.50 (10)	O(5)	0.433 (8)	0.328 (8)	0.733 (8)	0.46 (11)
O(2)	0.005 (8)	0.386 (8)	0.351 (9)	0.48 (10)	O(6)	0.400 (8)	0.127 (8)	0.548 (8)	0.49 (11)

[a] The form of the anisotropic thermal parameter (×10⁴) is $\exp[-2\pi^2(U_{11}h^2a^{*2} + U_{22}k^2b^{*2} + U_{33}l^2c^{*2} + 2U_{12}hka^*b^* + 2U_{13}hla^*c^* + 2U_{23}klb^*c^*)]$.

Table IV. Magnetic Data for the High-Pressure Polymorphs of $EuSiO_3$

phase	treatment: P, kbar	treatment: T, °C	μ_{eff},[a] μ_B	Θ_c,[b] K
α			7.95	−1
δ	60	1000	7.72	−3
δ′	70	1200	7.83	−3

[a] μ_{eff} = magnetic moment per Eu^{2+} ion. [b] Θ_c = paramagnetic Curie temperature. The measured range is 80–300 K.

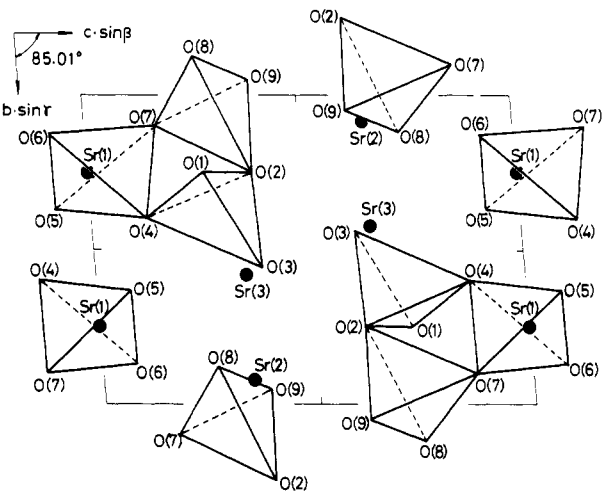

Figure 1. Projection of the δ-$SrSiO_3$ structure viewed along the *a* axis.

samples are paramagnetic down to low temperature, and thus the magnetic interactions between neighboring Eu^{2+} ions are weak.

Structures of δ- and δ′-$SrSiO_3$. The interatomic distances and angles of δ-$SrSiO_3$ are summarized in Table V, and the projection of its structure is shown in Figure 1. The atomic parameters of δ-$SrSiO_3$ (Table II) almost agree with those of δ-$CaSiO_3$ reported by Trojer,[9] where the *a*, *b*, and *c* axes of δ-$CaSiO_3$ correspond the −*a*, *c*, and *b* axes of δ-$SrSiO_3$, and

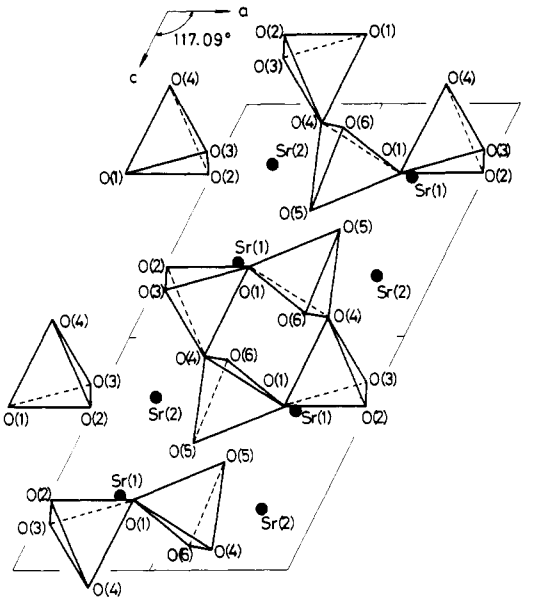

Figure 2. Projection of the δ′-$SrSiO_3$ structure viewed along the *b* axis.

hence the δ forms of $SrSiO_3$ and $CaSiO_3$ are isostructural. The structure of δ-$SrSiO_3$ consists of the same $(Si_3O_9)^{6-}$ rings as do the α forms of $CaSiO_3$ and $SrSiO_3$. The $(Si_3O_9)^{6-}$ ring is constructed of three distorted tetrahedra of $Si(1)O_4$, $Si(2)O_4$, and $Si(3)O_4$ by sharing the corner oxygens O(2), O(4), and O(7). Their Si–O bond lengths and angles vary from 1.50 to 1.74 Å and from 90.6 to 130.4°, respectively. Each Sr atom is surrounded by eight or six oxygens with Sr–O distances of 2.33–2.98 Å.

The interatomic distances and angles of δ′-$SrSiO_3$ are presented in Table VI, and the projection viewed along the *b* axis is illustrated in Figure 2. This silicate contains a four-membered $(Si_4O_{12})^{8-}$ ring, in which four tetrahedra are condensed by sharing O(1) and O(4) atoms. The $(Si_4O_{12})^{8-}$ ring has Si–O bond lengths ranging from 1.602 to 1.693 Å, O–Si–O bond angles from 103.1 to 116.0°, and an inversion

Table V. Interatomic Distances (Å) and Angles (Deg) for δ-$SrSiO_3$

(a) Si_3O_9 Ring Distances and Angles

	Si(1)-Tetrahedron		
Si(1)-O(1)	1.68 (1)	Si(1)-O(3)	1.52 (1)
Si(1)-O(2)	1.74 (1)	Si(1)-O(4)	1.51 (1)
		average	1.61
O(1)-Si(1)-O(2)	109.7 (6)	O(2)-Si(1)-O(3)	110.0 (6)
O(1)-Si(1)-O(3)	103.2 (6)	O(2)-Si(1)-O(4)	108.7 (6)
O(1)-Si(1)-O(4)	91.6 (7)	O(3)-Si(1)-O(4)	130.4 (7)
		average	109.0
	Si(2)-Tetrahedron		
Si(2)-O(4)	1.65 (1)	Si(2)-O(6)	1.59 (1)
Si(2)-O(5)	1.56 (1)	Si(2)-O(7)	1.65 (1)
		average	1.61
O(4)-Si(2)-O(5)	112.6 (7)	O(5)-Si(2)-O(6)	115.2 (6)
O(4)-Si(2)-O(6)	105.8 (6)	O(5)-Si(2)-O(7)	114.5 (6)
O(4)-Si(2)-O(7)	99.8 (6)	O(6)-Si(2)-O(7)	107.5 (6)
		average	109.2
	Si(3)-Tetrahedron		
Si(3)-O(2)	1.67 (1)	Si(3)-O(8)	1.63 (1)
Si(3)-O(7)	1.50 (1)	Si(3)-O(9)	1.57 (1)
		average	1.59
O(2)-Si(3)-O(7)	113.9 (9)	O(7)-Si(3)-O(8)	90.6 (6)
O(2)-Si(3)-O(8)	108.4 (6)	O(7)-Si(3)-O(9)	127.9 (7)
O(2)-Si(3)-O(9)	108.7 (6)	O(8)-Si(3)-O(9)	103.2 (6)
		average	108.8

(b) Sr-O Distances[a]

	Sr(1)-Polyhedron		
Sr(1)-O(1)	2.55 (1)	Sr(1)-O(6)	2.61 (1)
Sr(1)-O(4)	2.96 (1)	Sr(1)-O(6^{i})	2.66 (1)
Sr(1)-O(5)	2.67 (1)	Sr(1)-O(7^{i})	2.98 (1)
Sr(1)-O(5^{i})	2.60 (1)	Sr(1)-O(8^{i})	2.66 (1)
		average	2.71
	Sr(2)-Polyhedron		
Sr(2)-O(1^{i})	2.38 (1)	Sr(2)-O(8^{i})	2.33 (1)
Sr(2)-O(3^{i})	2.49 (1)	Sr(2)-O(9)	2.56 (1)
Sr(2)-O(6)	2.48 (1)	Sr(2)-O(9^{i})	2.48 (1)
		average	2.45
	Sr(3)-Polyhedron		
Sr(3)-O(1)	2.78 (1)	Sr(3)-O(5^{i})	2.53 (1)
Sr(3)-O(3)	2.56 (1)	Sr(3)-O(8)	2.69 (1)
Sr(3)-O(3^{i})	2.59 (1)	Sr(3)-O(9)	2.58 (1)
		average	2.62

[a] Symmetry transformations: O(n^{i}), ($\bar{x}$, $\bar{y}$, $\bar{z}$).

center. Such four-membered rings have been found to be contained in complex silicates,[17] but not in the other metasilicates except for δ′-$SrSiO_3$. The Sr atoms occupy the eightfold sites with the Sr–O distances varying from 2.409 to 3.058 Å. The structure of δ′-$SrSiO_3$ is constructed of Sr atoms and $(Si_4O_{12})^{8-}$ rings by packing along the *b* axis.

High-Pressure Polymorphisms of $SrSiO_3$ and $EuSiO_3$. The lattice parameters for the high-pressure phases of $CaSiO_3$, $SrSiO_3$, and $EuSiO_3$ are summarized in Table VII. The behavior for the phase transformation of $CaSiO_3$ differs somewhat from the cases of $SrSiO_3$ and $EuSiO_3$. The two phases α- and δ-$CaSiO_3$ correspond to the α and δ forms of $SrSiO_3$ and $EuSiO_3$, but the δ′ form is a phase that has not been observed in $CaSiO_3$. Since the ionic radii of Sr^{2+} and Eu^{2+} are almost equal to each other (see ref 18), both $SrSiO_3$ and $EuSiO_3$ can be seen to show the same high-pressure polymorphisms.

Luminescence Spectra of $CaSiO_3$:Eu^{2+} and $SrSiO_3$:Eu^{2+}. A series of high-pressure phases of $CaSiO_3$:Eu^{2+} and $SrSiO_3$:Eu^{2+} except for ε-$CaSiO_3$:Eu^{2+} were obtained by treatments at

(17) Wells, A. F. "Structural Inorganic Chemistry", 4th ed.; Oxford University Press: London, 1975; p 815.
(18) Shannon, R. D. *Acta Crystallogr., Sect. A* **1975**, *32*, 225.

Table VI. Interatomic Distances (Å) and Angles (Deg) for (Deg) for δ′-$SrSiO_3$

(a) Si_4O_{12} Ring Distances and Angles

	Si(1)-Tetrahedron		
Si(1)-O(1)	1.693 (9)	Si(1)-O(3)	1.624 (9)
Si(1)-O(2)	1.620 (9)	Si(1)-O(4)	1.622 (9)
		average	1.640
O(1)-Si(1)-O(2)	104.6 (5)	O(2)-Si(1)-O(3)	116.0 (5)
O(1)-Si(1)-O(3)	112.1 (5)	O(2)-Si(1)-O(4)	115.7 (5)
O(1)-Si(1)-O(4)	103.1 (5)	O(3)-Si(1)-O(4)	104.6 (5)
		average	109.4
	Si(2)-Tetrahedron		
Si(2)-O(1)	1.646 (9)	Si(2)-O(5)	1.636 (9)
Si(2)-O(4)	1.662 (9)	Si(2)-O(6)	1.602 (9)
		average	1.637
O(1)-Si(2)-O(4)	107.4 (5)	O(4)-Si(2)-O(5)	112.4 (5)
O(1)-Si(2)-O(5)	106.0 (5)	O(4)-Si(2)-O(6)	111.6 (5)
O(1)-Si(2)-O(6)	107.1 (5)	O(5)-Si(2)-O(6)	112.0 (5)
		average	109.4

(b) Sr-O Distances[a]

	Sr(1)-Polyhedron		
Sr(1)-O(1)	3.058 (9)	Sr(1)-O(3)	2.556 (8)
	3.054 (9)	Sr(1)-O(5^{iii})	2.409 (9)
Sr(1)-O(2)	2.648 (9)	Sr(1)-O(6)	2.510 (8)
Sr(1)-O(2^{ii})	2.721 (9)	Sr(1)-O(6^{i})	2.652 (8)
		average	2.701
	Sr(2)-Polyhedron		
Sr(2)-O(1^{iii})	2.714 (9)	Sr(2)-O(4)	2.627 (9)
Sr(2)-O(2^{i})	2.492 (9)	Sr(2)-O(5)	3.063 (9)
Sr(2)-O(3)	2.752 (8)	Sr(2)-O(5^{ii})	2.478 (9)
Sr(2)-O(3^{i})	2.496 (8)	Sr(2)-O(6)	2.503 (8)
		average	2.641

[a] Symmetry transformations: Sr(n^{i}) and O(n^{i}), ($\bar{x}$, $\bar{y}$, $\bar{z}$); Sr(n^{ii}) and O(n^{ii}), (x, $^1/_2 + y$, $^1/_2 - z$); Sr(n^{iii}) and O(n^{iii}), (x, $^1/_2 - y$, $^1/_2 + z$).

Table VII. Lattice Parameters for the High-Pressure Polymorphs of $MSiO_3$ (M = Ca, Sr, or Eu)

compd	parameter	α form	δ form	δ′ form	ε form
$CaSiO_3$	*a*, Å	6.90[a]	6.695 (5)[b]		
	b, Å	11.78	9.257 (7)		
	c, Å	19.65	6.666 (6)		3.485 (8)[c]
	α, deg	90.0	86.63 (5)		
	β, deg	90.8	76.13 (5)		
	γ, deg	90.0	70.38 (5)		
$SrSiO_3$	*a*, Å	12.323 (5)	6.874 (2)	7.452 (4)	
	b, Å	7.139 (2)	6.894 (2)	6.066 (2)	
	c, Å	10.873 (5)	9.717 (3)	13.479 (7)	
	α, deg		85.01 (3)		
	β, deg	111.58 (4)	110.57 (3)	117.09 (4)	
	γ, deg		104.01 (2)		
$EuSiO_3$	*a*, Å	12.337 (6)	6.877 (3)	7.455 (6)	
	b, Å	7.141 (3)	6.898 (3)	6.074 (4)	
	c, Å	10.894 (6)	9.727 (5)	13.513 (10)	
	α, deg		85.01 (4)		
	β, deg	111.58 (4)	110.58 (4)	117.19 (6)	
	γ, deg		104.00 (4)		

[a] Reference 8. [b] Reference 9. [c] Reference 6b.

35–100 kbar and 800–1400 °C. All of the obtained samples showed band emissions based on the $4f^7$–$4f^65d$ transitions of Eu^{2+} ions, and their luminescence properties varied considerably with the phase transformations. The emission and excitation spectra of $CaSiO_3$:Eu^{2+} (1 atom %) and $SrSiO_3$:Eu^{2+} (1 atom %) are shown in Figures 3 and 4, and the luminescence data are summarized in Table VIII.

The peak positions for the emission bands of the samples shift to short wavelength when the host lattices transform into high-pressure forms, δ-$CaSiO_3$ and δ′-$SrSiO_3$. The emission bands are centered at the following positions: 507 nm (green), α-$CaSiO_3$:Eu^{2+}; 472 nm (blue), δ-$CaSiO_3$:Eu^{2+}; 498 nm

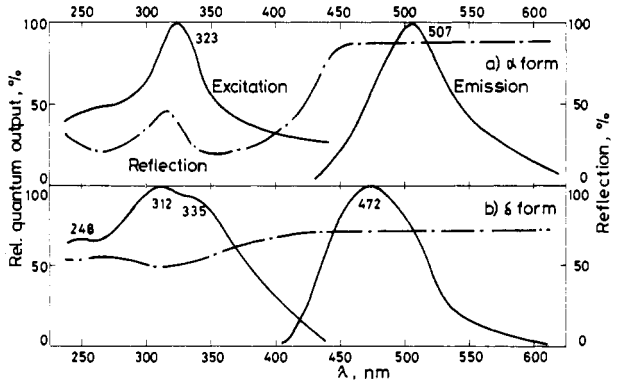

Figure 3. Relative emission and excitation spectra (solid lines) and diffuse reflection spectra (dashed–dotted lines) for α- and δ-$CaSiO_3$:Eu^{2+} (1 atom %) phosphors.

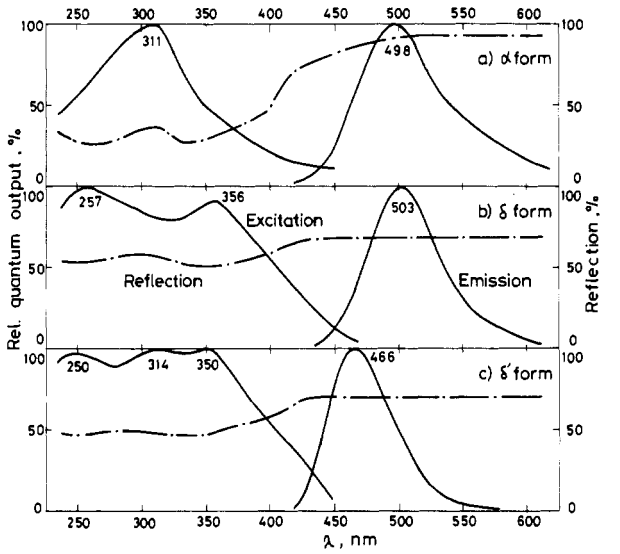

Figure 4. Relative emission and excitation spectra (solid lines) and diffuse reflection spectra (dashed–dotted lines) for the high-pressure polymorphs of $SrSiO_3$:Eu^{2+} (1 atom %) phosphor.

Table VIII. Luminescence Data for the High-Pressure Polymorphs of $CaSiO_3$:Eu^{2+} (1 atom %) and $SrSiO_3$:Eu^{2+} (1 atom %)

phase	treatment		λ_{max},[a] nm	$\lambda/2$,[b] nm	% QE[c]	T_{50},[d] K
	P, kbar	T, °C				
α-$CaSiO_3$			507	70–80	≃1	420
δ-$CaSiO_3$	45	1000	472	83	22	420
α-$SrSiO_3$			498	75–80	<1	380
δ-$SrSiO_3$	35	1000	503	63	6	300
δ'-$SrSiO_3$	60	1000	466	58	37	360

[a] λ_{max} = peak position of the emission band at 300 K. [b] $\lambda/2$ = half-width of emission band. [c] QE = quantum efficiency under an optimum excitation at 300 K. [d] T_{50} = quenching temperature at which the intensity of the luminescence is half of that at 77 K.

(green), α-$SrSiO_3$:Eu^{2+}; 503 nm (green), δ-$SrSiO_3$:Eu^{2+}; 466 nm (blue), δ'-$SrSiO_3$:Eu^{2+}.

The excitation spectrum patterns of samples consist of a band peaking at 311 or 323 nm for α-$CaSiO_3$:Eu^{2+} or α-$SrSiO_3$:Eu^{2+}, two bands peaking at 257 and 356 nm for δ-$SrSiO_3$:Eu^{2+}, and three bands peaking at 248, 312, and 335 nm or 250, 314, and 350 nm for δ-$CaSiO_3$:Eu^{2+} or δ'-$SrSiO_3$:Eu^{2+}. For the compounds containing Eu^{2+} ions, the absorptions in the near-ultraviolet region are attributable to the 4f → 5d transitions of Eu^{2+} ions.[19] Therefore, the absorption (reflection) spectrum patterns of the samples are

(19) McClure, D. S.; Kiss, Z. J. *J. Chem. Phys.* **1963**, *39*, 3251.

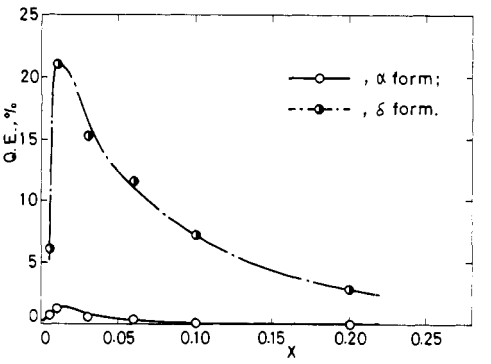

Figure 5. Quantum efficiency vs. Eu^{2+} content, x, for α and δ phases of $Ca_{1-x}Eu_xSiO_3$.

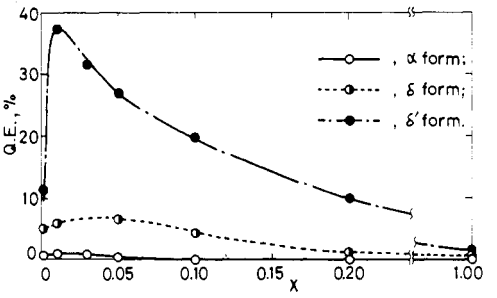

Figure 6. Quantum efficiency vs. Eu^{2+} content, x, for the high-pressure polymorphs of $Sr_{1-x}Eu_xSiO_3$.

generally compatible with their excitation spectrum patterns. The reflection spectra for δ-$CaSiO_3$:Eu^{2+}, δ-$SrSiO_3$:Eu^{2+}, and δ'-$SrSiO_3$:Eu^{2+} can be seen from Figures 3 and 4 to correspond to the excitation spectra, but the excitation spectrum patterns of α-$CaSiO_3$:Eu^{2+} and α-$SrSiO_3$:Eu^{2+} are not compatible with the reflection spectrum patterns, which consist of two absorption bands around 270 and 350 nm. From this observation, we can presume that there are two kinds of Eu^{2+} ions in α-$CaSiO_3$:Eu^{2+} and α-$SrSiO_3$:Eu^{2+}; that is, one acts as the luminescence center but the other does not contribute to the luminescence. If most of the Eu^{2+} ions in the samples belong to the latter type, we should observe only absorption (reflection) patterns for this type of Eu^{2+} ion. The small amount of Eu^{2+} ions must be classified as the former type and contributes to the luminescence but not to the overall observable absorption spectrum.

The emission intensities (quantum efficiencies) of $CaSiO_3$:Eu^{2+} and $SrSiO_3$:Eu^{2+} were also found to increase appreciably 20–40 times with shifts for the peak positions of the emission bands when the host lattices transform into δ-$CaSiO_3$ and δ'-$SrSiO_3$. While the quantum efficiencies of α phases are very weak (QE ≃ 1%), their high-pressure phases give relatively high quantum efficiency values (under optimum Eu^{2+} concentrations and excitations): 22%, δ-$CaSiO_3$:Eu^{2+}; 7%, δ-$SrSiO_3$:Eu^{2+}; 37%, δ'-$SrSiO_3$:Eu^{2+}. The concentration dependences for quantum efficiencies of samples are summarized in Figures 5 and 6. The optimum concentration of Eu^{2+} ions for the luminescence is around 1–2 atom % for α-$CaSiO_3$:Eu^{2+}, 1 atom % for δ-$CaSiO_3$:Eu^{2+}, 2 atom % for α-$SrSiO_3$:Eu^{2+}, 4 atom % for δ-$SrSiO_3$:Eu^{2+}, and 1 atom % for δ'-$SrSiO_3$:Eu^{2+}, respectively.

The temperature dependences for the emission intensities of the samples are shown in Figures 7 and 8. The light output at 77 K was adopted as a standard for the temperature dependence of each sample. The quenching curves of α-$CaSiO_3$:Eu^{2+} and δ-$CaSiO_3$:Eu^{2+} can be seen to be closely similar to each other, and both of these phases give T_{50} = 420 K (Table VIII). The shape for the quenching curve of α-$SrSiO_3$:Eu^{2+} differs from that of δ- and δ'-$SrSiO_3$:Eu^{2+}. The

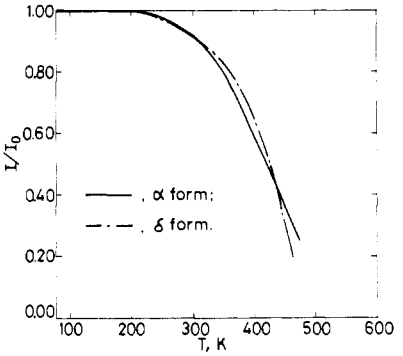

Figure 7. Temperature dependences of the light output for α and δ phases of $CaSiO_3:Eu^{2+}$ (1 atom %).

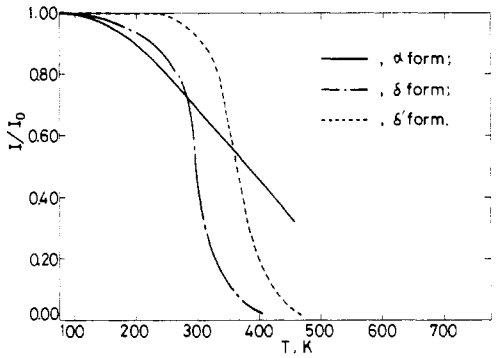

Figure 8. Temperature dependences of the light output for the high-pressure polymorphs of $SrSiO_3:Eu^{2+}$ (1 atom %).

Table IX. X-ray Powder Diffraction Data for $CaSiO_3:Eu^{2+}$ (1 atom %) and ϵ-$CaSiO_3$

$CaSiO_3:Eu^{2+}$					
d_{obsd}, Å	I/I_0	d_{obsd}, Å	I/I_0	d_{obsd}, Å	I/I_0
3.03	100	2.52	55	2.04	35
2.92	75	2.44	50	2.02	25
2.79	95	2.40	30	1.98	50
2.75	65	2.28	30	1.89	20
2.69	35	2.19	55	1.63	30
2.61	50	2.12	30	1.60	30
ϵ-$CaSiO_3$[a]					
d_{obsd}, Å	I/I_0	d_{obsd}, Å	I/I_0	d_{obsd}, Å	I/I_0
2.467	100	1.742	80	1.427	60
2.009	60	1.570	5	1.229	50

[a] Reference 6b.

T_{50} values are 380, 300, and 360 K for the α, δ, and δ' forms, respectively. However, the data of the α form seem to be unreliable because its emission intensity is weak.

Ringwood and Major[20] have pointed out that the perovskite modification of $CaSiO_3$ (ϵ form) is formed under pressures exceeding 100 kbar, but on the release of pressure, it retrogressively transformed to either glass, ϵ-$CaSiO_3$, or mixtures of these phases. For $CaSiO_3:Eu^{2+}$, however, instead of ϵ-$CaSiO_3$ or the vitreous phase, which are expected to be obtained by the treatments of α-$CaSiO_3:Eu^{2+}$ at 150 kbar and 1000 °C, an unknown phase was obtained. Its X-ray powder diffraction data are presented together with the data of ϵ-$CaSiO_3$ in Table IX.

The stability for the perovskite type structure of ABO_3 oxides (A, large cation; B, small cation) can be estimated from the tolerance factor t. In Table X, the t values for some silicates $MSiO_3$ (M = Ca, Sr, or Eu) are summarized. When

(20) Ringwood, A. E.; Major, A. *Earth Planet. Sci. Lett.* **1971**, *12*, 411.

Table X. Tolerance Factors for Perovskite Modifications of $MSiO_3$ (M = Ca, Sr, or Eu)

compd	t[a]
$CaSiO_3$	1.08
$SrSiO_3$	1.12
$EuSiO_3$	1.11

[a] $t = (r_A + r_B)/[2^{1/2}(r_B + r_X)]$, where the values of r_A, r_B, and r_X represent the ionic radii of M^{2+}, Si^{4+}, and O^{2-}, the values of which are given in ref 18.

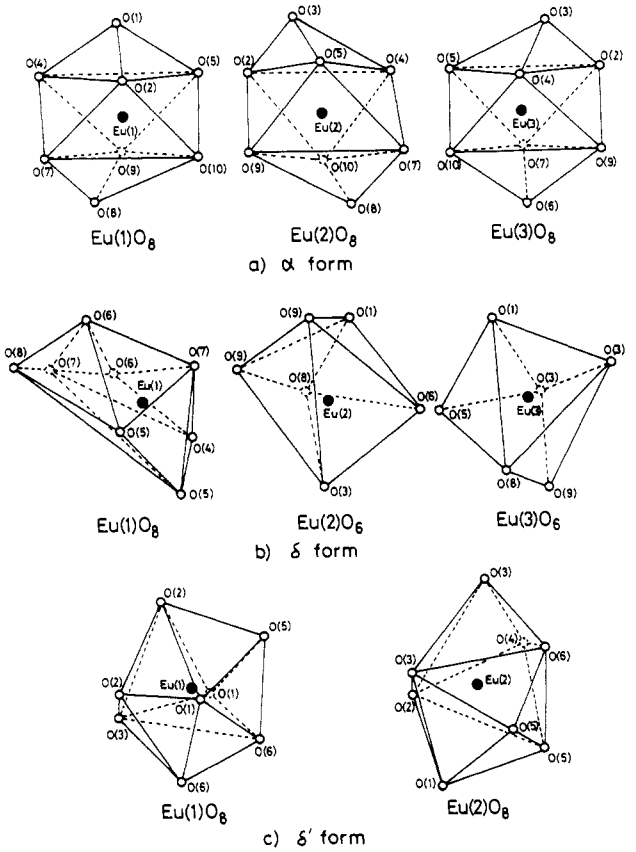

Figure 9. Schematic illustrations of the EuO_n polyhedra in the high-pressure polymorphs of the $SrSiO_3:Eu^{2+}$ phosphor.

the value of t is between 0.89 and 1.00, in general, the cubic perovskite modification is formed. $CaSiO_3$, $SrSiO_3$, and $EuSiO_3$ all give larger values of t than 1.00. It is impossible for these silicates to obtain the perovskite modifications. From the experimental results,[6b] however, $CaSiO_3$, whose t value is the smallest among them, has been found to be barely transformed into the ϵ form by the treatments at very high pressures, but, from their large values of t, both $SrSiO_3$ and $EuSiO_3$ can not be expected to give the ϵ phase. Therefore, the experimental observation that the perovskite modification of $CaSiO_3:Eu^{2+}$ has not been obtained by the treatment at 150 kbar must be responsible for the large Eu^{2+} ions in the matrix of $CaSiO_3$.

Discussion

Since the absorption (excitation) spectra in Eu^{2+}-activated phosphors are attributable to the 4f → 5d transitions of Eu^{2+} ions, their spectrum patterns reflect splittings of 5d levels by the crystal fields. The Eu^{2+} ions in $CaSiO_3:Eu^{2+}$ and $SrSiO_3:Eu^{2+}$ phosphors occupy the sites of Ca^{2+} and Sr^{2+} ions. In Figure 9, we illustrate the oxygen arrangements around the Eu^{2+} ions in $SrSiO_3:Eu^{2+}$ polymorphs. The α and δ phases of $CaSiO_3$ or $SrSiO_3$ are approximately or entirely isostructural with the corresponding analogues, and hence the anion environments of the Eu^{2+} ions in $CaSiO_3:Eu^{2+}$ are closely similar to those in $SrSiO_3:Eu^{2+}$. The symmetries of these polyhedra

Table XI. Oxygen Arrangements around Sr Atoms in the High-Pressure Polymorphs of $CaSiO_3$ and $SrSiO_3$

phase	site	CN[a]	mean M–O dist, Å
α-$CaSiO_3$[b]	Ca	8	
δ-$CaSiO_3$[c]	Ca(1)	8	2.630
	Ca(2)	6	2.467
	Ca(3)	6	2.375
α-$SrSiO_3$[d]	Sr(1)	8	2.68
	Sr(2)	8	2.65
	Sr(3)	8	2.60
δ-$SrSiO_3$	Sr(1)	8	2.71
	Sr(2)	6	2.45
	Sr(3)	6	2.62
δ'-$SrSiO_3$	Sr(1)	8	2.701
	Sr(2)	8	2.641

[a] CN = M (Ca or Sr) coordination number to oxygens. [b] The detailed structural analysis of this form has not been performed. [c] Reference 9. [d] Reference 11.

are very low (point group $C1$), although the EuO_8 polyhedra in α-$SrSiO_3$:Eu^{2+} have symmetry similar to that of a polyhedron with point group Ci. It may be difficult, therefore, to assign exactly the excitation spectrum patterns on the basis of the splittings of 5d levels by the crystal fields.

The Eu^{2+} ions in δ'-$SrSiO_3$:Eu^{2+}, which are surrounded by eight oxygens, give an excitation spectrum consisting of three bands (Figure 4). This observation means that the $Eu(1)O_8$ and $Eu(2)O_8$ polyhedra shown in Figure 9 form the crystal field by which the 5d level is split into three levels.

For the α phases of $CaSiO_3$:Eu^{2+} and $SrSiO_3$:Eu^{2+}, the Eu^{2+} ions occupy the eightfold sites to form EuO_8 polyhedra similar to those in δ'-$SrSiO_3$:Eu^{2+}. Thus these phosphors can also be expected to give the same crystal fields around Eu^{2+} ions as δ'-$SrSiO_3$:Eu^{2+}. However, the estimated excitation spectrum profile agrees with the reflection spectra, but not with their excitation spectra. It is concluded that the Eu^{2+} ions placed on the eightfold sites in α-$CaSiO_3$ and α-$SrSiO_3$ cannot give the luminescence and contribute only to the absorption in the near-ultraviolet region. The Eu^{2+} ions responsible for the luminescence centers must be located on positions different from the above-mentioned eightfold sites, e.g., grain boundary or vitreous regions in the matrix.

For δ-$SrSiO_3$:Eu^{2+}, the Eu^{2+} ions are surrounded by eight or six oxygens to form $Eu(1)O_8$, $Eu(2)O_6$, and $Eu(3)O_6$ polyhedra. Among them, the EuO_6 octahedra give a different crystal field from that of EuO_8 polyhedra, by which the 5d level of the Eu^{2+} ion is split into two levels of e_g and t_{2g}, roughly speaking, because the symmetries of the $Eu(2)O_6$ and $Eu(3)O_6$ octahedra are similar to that of the regular octahedron. As two-thirds of the Eu^{2+} ions statistically occupy the sixfold sites of Sr(2) and Sr(3) atoms in δ-$SrSiO_3$, this phosphor apparently gives the excitation spectrum of two bands peaking at 257 and 356 nm.

The δ phase of $CaSiO_3$:Eu^{2+}, which is isostructural with δ-$SrSiO_3$:Eu^{2+}, is expected to give an excitation spectrum with two maxima, but its spectrum pattern consists of three bands like that of δ'-$SrSiO_3$:Eu^{2+}. This can be interpreted from the difference in the ionic radii of Ca^{2+}, Sr^{2+}, and Eu^{2+}. The ionic radius of Eu^{2+} is almost equal to that of Sr^{2+}, but it is larger than that of Ca^{2+}. Thus the Eu–O and Sr–O distances should be long compared with the Ca–O length. The mean Ca–O and Sr–O distances in $CaSiO_3$ and $SrSiO_3$ polymorphs are presented in Table XI. For δ-$CaSiO_3$, the Ca–O distance of the Ca(1) site (2.630 Å) is longer than those of Ca(2) and Ca(3) sites and is comparable to the normal Sr–O or Eu–O distance (2.60–2.70 Å). In δ-$CaSiO_3$:Eu^{2+}, consequently, most of the Eu^{2+} ions are located on the eightfold site of the Ca(1) atom rather than the sixfold sites of Ca(2) and Ca(3) atoms, and hence this phosphor must give the same excitation spectrum pattern as δ'-$SrSiO_3$:Eu^{2+}.

Table XII. Interatomic Distances between the Eu Neighbors in the High-Pressure Polymorphs of $SrSiO_3$:Eu^{2+}

phase	site	mean Eu–Eu dist,[a] Å	
		nn	nnn
α-$SrSiO_3$[b]	Eu(1)	4.12 (×6)	5.08 (×2)
	Eu(2)	4.12 (×6)	5.07 (×2)
	Eu(3)	4.12 (×6)	5.04 (×2)
δ-$SrSiO_3$	Eu(1)	3.89 (×4)	4.24 (×2)
	Eu(2)	3.88 (×3)	4.41 (×2)
	Eu(3)	3.85 (×4)	4.41 (×2)
δ'-$SrSiO_3$	Eu(1)	4.03 (×6)	4.62 (×1)
	Eu(2)	3.92 (×6)	5.05 (×1)

[a] nn and nnn represent the nearest and next-nearest Eu neighbors, respectively. [b] These distances are calculated on the basis of the atomic coordinates of α-$SrSiO_3$ reported in ref 11.

The peak positions for emission bands of Eu^{2+}-activated phosphors also depend on the arrangements of the anions around Eu^{2+} ions, the electronegativity of anions, etc. Both δ-$CaSiO_3$:Eu^{2+} and δ'-$SrSiO_3$:Eu^{2+}, in which the Eu^{2+} ions must occupy the eightfold sites with similar Eu–O distances to each other, show the same emissions around 470 nm, whereas the Eu^{2+} ions placed on the eightfold and sixfold sites in δ-$SrSiO_3$:Eu^{2+} give the emission band peaking at about 510 nm.

It is noticeable that the quantum efficiencies of $CaSiO_3$:Eu^{2+} and $SrSiO_3$:Eu^{2+} appreciably increase when the host lattices transform into the high-pressure phases. Since the constituent chemical species of the samples are unchangeable throughout the phase transformations, the differences in their quantum efficiencies are qualitatively interpreted by considering the crystal structures.

Repeats of the energy transfers via Coulomb and exchange interactions between neighboring Eu^{2+} ions are pointed out as one of the quenching effects on Eu^{2+}-activated phosphors. The critical distance R_c for most of them is 20–25 Å for the Coulomb interaction and 4–5 Å for the exchange interaction, where R_c represents the distance between two luminescent centers, S (sensitizer) and A (activator) at which the probability of transfer from S to A is equal to the probability of radiative emission of S. The Eu^{2+} ions in Eu^{2+}-activated phosphors act as both S and A. The magnitudes of the above-mentioned interactions can be estimated from the proportion of overlap between the absorption (reflection) and emission bands and depend on the number of neighboring Eu^{2+} ions and their interatomic distances. The distances between the neighboring sites that can be occupied by the Eu^{2+} ions in $SrSiO_3$:Eu^{2+} polymorphs are summarized in Table XII. The mean distances are 3.85–4.12 Å for the nearest Eu neighbors and 4.24–5.08 Å for the next-nearest Eu neighbors, respectively. These distances suffice for the energy transfer.

From the reflection spectrum measurements of the samples (Figures 3 and 4), generally speaking, the overlaps between the reflection and emission bands are small. Thus, energy transfers between the neighboring Eu^{2+} ions do not occur so often. However, α-$CaSiO_3$:Eu^{2+} or α-$SrSiO_3$:Eu^{2+} has a great absorption band at 320–450 nm, and consequently, if the Eu^{2+} ions that occupy the eightfold sites give the emission around 470 nm like δ-$CaSiO_3$:Eu^{2+} or δ'-$SrSiO_3$:Eu^{2+}, the overlaps between their absorption and emission spectra will be great. This assumption sufficiently suggests that no luminescence is caused by the Eu^{2+} ions placed on the eightfold sites, and emission spectra (507 and 498 nm) that hardly overlap with the absorption bands are observable.

On the basis of the measurements of quenching temperature, we can estimate the effect of lattice vibrations on the luminescence. The experimental result that the T_{50} value of δ'-$SrSiO_3$:Eu^{2+} (ca. 360 K) is high compared with that of

δ-$SrSiO_3$:Eu^{2+} (ca. 300 K) means that the quenching effect via lattice vibrations of $(Si_3O_9)^{6-}$ rings is greater than that of $(Si_4O_{12})^{8-}$ rings. Therefore, δ'-$SrSiO_3$:Eu^{2+} gives an emission with high quantum efficiency compared with δ-$SrSiO_3$:Eu^{2+}.

The Eu^{2+} ions in δ-$CaSiO_3$:Eu^{2+} must selectively occupy the eightfold sites rather than the sixfold sites. As the dispersion of the Eu^{2+} ions in the matrix is expected to be good, the quenching effect of the energy transfer seems to be smaller than that of δ-$SrSiO_3$:Eu^{2+}. The great T_{50} value (ca. 420 K) indicates that the quenching effect of lattice vibration is relatively small. We can interpret from these considerations that δ-$CaSiO_3$:Eu^{2+} gives strong emission similar to δ'-$SrSiO_3$:Eu^{2+} in spite of the crystallographic mismatch between Ca^{2+} and Eu^{2+} ions.

Conclusion

Both $SrSiO_3$ and $EuSiO_3$ show similar high-pressure polymorphisms to that of $CaSiO_3$ and transform into the δ and δ' phases at a pressure of 35–70 kbar. The δ form is isostructural with δ-$CaSiO_3$, but the δ' phase is not formed for $CaSiO_3$, and hence it is a phase characteristic of $SrSiO_3$ or $EuSiO_3$. The ϵ (perovskite) form of $SrSiO_3$ or $EuSiO_3$ is not obtained because of the large ionic radius of Sr^{2+} or Eu^{2+}. The structures of δ-$SrSiO_3$ and δ-$EuSiO_3$ consist of $(Si_3O_9)^{6-}$ rings in a similar manner as δ-$CaSiO_3$ while δ'-$SrSiO_3$ and δ'-$EuSiO_3$ contain $(Si_4O_{12})^{8-}$ rings. The Sr or Eu atoms in these phases are surrounded by eight or six oxygens for the δ form and eight oxygens for the δ' form.

The luminescence properties of $CaSiO_3$:Eu^{2+} and $SrSiO_3$:Eu^{2+} phosphors change considerably following the phase transformations. The excitation and emission spectra of δ-$CaSiO_3$:Eu^{2+} and δ'-$SrSiO_3$:Eu^{2+} are responsible for the Eu^{2+} ions that occupy the eightfold sites in the matrices while the Eu^{2+} ions on the eightfold and sixfold sites in δ-$SrSiO_3$:Eu^{2+} contribute to its luminescence spectra. For the α phases of $CaSiO_3$:Eu^{2+} and $SrSiO_3$:Eu^{2+}, the reflection spectra disagree with their excitation spectrum patterns. This means that there are two kinds of Eu^{2+} ions in the matrices: one contributes as the luminescence center whereas the other does not. Most of the Eu^{2+} ions belong to the latter type, and hence the emission intensity of this phase is weak. The experimental observation that the quantum efficiency of the sample appreciably increases with transformation into the δ-$CaSiO_3$ or δ'-$SrSiO_3$ phase is qualitatively interpreted by considering the crystal structure of the host lattice and the dispersion of Eu^{2+} ions in the matrix.

Acknowledgment. This work was supported by a grant from The Asahi Glass Foundation for Industrial Technology for G. A. The authors wish to thank Mr. N. Ogawa for the preparation of samples, Mr. M. Setoguchi for the measurements of the four-circle X-ray diffractometer, and Drs. N. Kasai, N. Yasuoka, and K. Miki for their valuable suggestions on X-ray analyses. The computations were carried out on an ACOS Series 77 NEAC System 700 computer at the Crystallographic Research Center, Institute for Protein Research, Osaka University.

Registry No. $EuSiO_3$, 15060-38-5; $CaSiO_3$, 10101-39-0; $SrSiO_3$, 13451-00-8.

Supplementary Material Available: Listing of observed and calculated structure factor amplitudes (7 pages). Ordering information is given on any current masthead page.

Contribution from the Chemistry Department, University of Virginia, Charlottesville, Virginia 22901

Matrix Infrared Spectra of the NCl_2 and NBr_2 Free Radicals

CHRISTOPHER K. KOHLMILLER and LESTER ANDREWS*

Received October 2, 1981

Mixtures of argon/chlorine/nitrogen were passed through a microwave discharge and condensed on a 15 K substrate. In addition to the NCl doublet at 823.5 and 817.2 cm^{-1}, a sharp new absorption with 9/6/1 relative intensity splittings appeared at 679.1, 677.4, and 675.8 ± 0.2 cm^{-1}. A nitrogen-15-enriched experiment produced a doublet of triplets and provided the NCl_2 identification and a 111 ± 4° calculation of the valence angle. Similar experiments with argon/bromine/nitrogen mixtures produced a sharp 603.5-cm^{-1} absorption with the appropriate nitrogen-15 shift for NBr_2.

Introduction

Much work has been done on electrical discharges in nitrogen since they were first reported in 1884,[1] and several reviews of their physical and chemical properties have appeared.[1-3] Experience has shown that these electrical discharges, microwave and radio frequency, are the only practical sources of nitrogen atoms in the gas phase. Ground-state nitrogen atoms are probably the main reactive species in "active" nitrogen,[2] as the discharge gas is often called, but other species, including vibrationally excited ground-state N_2 molecules and electronically excited N_2 molecules ($A^3\Sigma_u^+$), are present, and may also be significant.[4] Reactions of nitrogen atoms with other molecules in discharges have been studied, including the reaction with halogen molecules.[4] Raxworthy and Phillips[5] formed NCl and NBr in N_2 discharges with Cl_2 and Br_2. Using this approach, Miller and Andrews[6] trapped NCl, NBr, and NI in solid argon for laser-induced fluorescence study by condensing the effluent from an argon discharge containing the elements. The first identification of NCl_2 was provided by Briggs and Norrish[7] from flash photolysis of a NCl_3 and Cl_2 mixture. Clark and Clyne[8] later studied kinetics of the NCl_2 radical through the disappearance of a transient absorption at 299 nm; these workers prepared NCl_2 by reacting NCl_3 with Cl atoms from a microwave discharge. The NCl_2 radical has also been observed in the decomposition of NCl_3 in a helium atmosphere at room temperature,[9] and the matrix ESR spectrum of NCl_2 has been

(1) McTaggart, F. K. "Plasma Chemistry in Electrical Discharges"; Elsevier: Amsterdam, 1967; Chapter 8.
(2) Brocklehurst, B.; Jennings, K. R. In "Progress in Reaction Kinetics"; Porter, G., Ed.; Pergamon Press: Oxford, 1967; Vol. IV.
(3) Mannella, G. G. *Chem. Rev.* **1963**, *63*, 1.
(4) White, J. M. In "Comprehensive Chemical Kinetics"; Bamford, C. H., Tipper, C. F. H., Eds.; Elsevier: Amsterdam, 1972; Vol. 6.
(5) Raxworthy, K. S.; Phillips, L. F. *Can. J. Chem.* **1964**, *42*, 2928.
(6) Miller, J. C.; Andrews, L. *J. Chem. Phys.* **1979**, *71*, 5276.
(7) Briggs, A. G.; Norrish, R. G. W. *Proc. R. Soc., London* **1964**, *278*, 27.
(8) Clark, T. C.; Clyne, M. A. A. *Trans. Faraday Soc.* **1969**, *65*, 2994.

0020-1669/82/1321-1519$01.25/0